The Temperature Dependence of Salt−Protein Association Is Sequence Specific†

Liang Ma‡ and Qiang Cui*,‡,§

Graduate Program in Biophysics, Department of Chemistry, and Theoretical Chemistry Institute, University of Wisconsin, Madison, Wisconsin 53706

Received June 29, 2006; Revised Manuscript Received September 15, 2006

ABSTRACT: Molecular dynamics (MD) simulations are used to probe the origin of the unexpected temperature dependence of salt accumulation in the C-terminal region of the protein human lymphotactin. As in previous MD simulations, sodium ions accumulate in an enhanced manner near the C-terminal helix at the lower temperature, while the temperature dependence of chloride accumulation is much weaker and slightly positive. In a designed mutant in which all positively charged residues in the C-terminal helix are replaced with neutral polar groups (Ser), the unexpected temperature dependence of the sodium ions is no longer observed. Therefore, these simulations convincingly verified the previous hypothesis that the temperature dependence of ion−protein association is sensitive to the local sequence. This is explained qualitatively in terms of the entropy of association between charged species in solution. These findings have general implications for the interpretation of thermodynamic quantities associated with binding events where ion release is important, such as protein−DNA interactions.

Biomolecules exist in a heterogeneous cellular environment to play their functional roles. It has been widely recognized that environmental factors such as temperature and the presence of small solutes and ions can influence the conformational stabilities of biomolecules and therefore their function (*1*−*3*). For example, a vast amount of literature has shown that different salt ions preferentially stabilize the native or denatured state of proteins and therefore modulate the folding−unfolding equilibrium (*4*−*7*). Weak solute effects have also been proposed to be relevant to the long-range communication of biomolecules in cellular environments (*2*). A quantitative theory that is capable of predicting the effect of identity and concentration of small solutes on the structure and stability of biomolecules, however, is not yet available. Therefore, it is of interest to employ atomistic simulations in revealing detailed descriptions for the interaction between biomolecules and small solutes as well as how the interaction depends on environmental variables such as temperature. The insights will provide essential clues regarding the molecular mechanism that biomolecules employ to respond and adapt to environmental variations.

A remarkable example in this context is the human lymphotactin (hLtn).[1] Recent NMR experiments have shown that hLtn converts between two distinct folds under different salt and temperature conditions, and it also tends to dimerize under the high-temperature (∼45 °C) and low-salt condition (*8*). In our recent molecular dynamics (MD) simulation study of hLtn (*9*), an intriguing finding is that sodium ions, and chloride to a lesser degree, tend to strengthen their association with the C-terminal region of hLtn as the temperature decreases. This is unexpected since the dehydration free energies of both ions and charged side chains are lower at higher temperatures, and thus, ion−protein association is expected to be stronger at the higher temperature (*10*), which is indeed what was observed for most regions of hLtn except the C-terminal helix. Thus, the result hinted at the sequence sensitivity for the temperature dependence of ion−protein association, although the influence from other factors such as structural fluctuations could not be ruled out (*9*).

A specific hypothesis raised in that study (*9*) is that the unexpected temperature dependence is due to the presence of residues of mixed charges in the C-terminal region (see below). To explicitly test this hypothesis without other complicating factors, we carry out MD simulations for the hLtn C-terminal helix itself and a designed mutant. The wild-type sequence is ATWVREVVRSMDRKSN (charged residues are underlined) with a net charge of +2. In the mutant, all positively charged residues are replaced with neutral polar residues, resulting in the sequence ATWVSEVVSSMDSSSN with a net charge of −2. The expectation of the design is that the unusual temperature dependence of the salt−peptide association is observed only in the wild type and not in the mutant peptide.

METHODS

Molecular Dynamics Simulations. All simulations are carried out using CHARMM (*11*). The starting structure for the wild-type C-terminal helix is taken from the NMR structure of hLtn (PDB entry 1J9O). For the designed mutant, the side chains of positively charged residues are replaced with that of serine. The peptide is solvated in a rhombic dodecahedron solvent box, and sodium and chloride ions are added to keep the charge neutrality of the system with an approximate concentration of 200 mM. The simulation setup

† This work is partially supported by a grant from the National Institutes of Health (R01-GM071428-02). Q.C. is an Alfred P. Sloan Research Fellow.

* To whom correspondence should be addressed. E-mail: cui@chem.wisc.edu.
‡ Graduate Program in Biophysics.
§ Department of Chemistry and Theoretical Chemistry Institute.

[1] Abbreviations: MD, molecular dynamics; hLtn, human lymphotactin; PB, Poisson−Boltzmann.

10.1021/bi0613067 CCC: $33.50
Published on Web 11/07/2006

Table 1: Simulation Setup for All Molecular Dynamics Calculations

system	state[a]	no. of Cl^- ions	no. of Na^+ ions	average box length[b] (Å)	simulation time (ns)
wild-type	s10	10	8	47.7	23
wild-type	s45	10	8	48.2	23
mutant	s10	8	10	47.7	23
mutant	s45	8	10	48.2	24

[a] s10 and s45 refer to a salt condition where the NaCl concentration is 200 mM at 10 and 45 °C, respectively. [b] The average box lengths are for the rhombic dodecahedron periodic system.

details are listed in Table 1. The SHAKE algorithm (*12*) is used to allow an integration time step of 2 fs. A switching (*13*) scheme for interatomic distances between 10 and 12 Å is used for van der Waals interactions. For electrostatic interactions, the particle mesh Ewald scheme (*14*) is used. After the system is assembled, heating is carried out with the peptide atoms harmonically restrained using a force constant of 40 kcal mol^{-1} $Å^{-2}$. Equilibration for 20 ps and ~23 ns production runs are performed with a constant temperature and pressure; peptide backbone atoms are always harmonically restrained to avoid large structural variations, thus minimizing the number of variables that affect the ion−peptide association. The temperature is controlled using the Nose−Hoover algorithm (*15*, *16*), using a mass of 250 kcal/ps^2 for the thermostat and a reference temperature equal to the desired system temperature (10 or 45 °C). The pressure is controlled with the Anderson algorithm (*17*, *18*), using a mass of 500 amu for the pressure piston, a reference pressure of 1 atm, a Langevin piston collision frequency of 10 ps^{-1}, and a Langevin piston bath temperature equal to the desired system temperature.

Calculation Methods for the Radial Distribution Function g(r) and Its Integration N(r) Based on MD Simulations. For the calculations of the ion−peptide−surface radial distribution function, $g(r)$, the shortest distances between a specific type of ion (sodium or chloride) and the peptide atoms are collected from MD simulation trajectories and binned $[\delta N(r)]$. The volume factor (δV) corresponding to the bin (r, dr) is estimated using the volume function in CHARMM (COOR VOLU) with all the peptide atoms (irrespective of atom type) having a radius of either $r + dr/2$ or $r - dr/2$; i.e., $\delta V = V(r + dr/2) - V(r - dr/2)$. The ion−surface radial distribution function is then calculated as

$$g(r) = \frac{\delta N(r)}{\delta V(r)\rho_\infty}\frac{1}{} \qquad (1)$$

where the "bulk number density" (ρ_∞) is estimated by dividing the number of ions by the average volume of the simulation box.

The radial distribution functions are also integrated over the distance from the peptide surface to provide a more explicit description for the average number of ions $[N(r)]$ that accumulated around the peptide.

Nonlinear Poisson−Boltzmann (PB) Calculations. Nonlinear Poisson−Boltzmann calculations are also carried out in an effort to explore the temperature dependence of ion−protein association and to compare it with MD simulations. Peptide snapshots are collected from the explicit simulations, and the ion distributions at different temperatures are calculated. The set of atomic radii established by Roux and co-workers (*19*) is used together with a solvent probe radius of 1.4 Å and a stern ion-exclusion layer of 2 Å. The partial charges are those in the standard CHARMM 22 force field for proteins (*20*). The grid consists of 201^3 points spaced by 0.2 Å. With respect to the value of the dielectric constant, a value of 2 is used for the protein and assumed to be independent of temperature. The dielectric constant of bulk water, however, is taken as a function inversely dependent on temperature (*10*); specifically, the value is 83.9 and 71.6 at 10 and 45 °C, respectively.

Once the electrostatic potential is solved using PB, the ion distribution can be obtained with the Debye−Hückel expression

$$\rho_{Na^+/Cl^-}(\vec{r}) = \rho_\infty \exp[-\beta q_{Na^+/Cl^-}\phi(\vec{r})] \qquad (2)$$

where ρ_∞ is the bulk salt concentration, β the inverse temperature, and q the charge of a specific type of ion.

Multiple-Sequence Alignment. Multiple-sequence alignment for several hLtn orthologs in different organisms is performed using MUSCLE (*21*), and the sequence conservation in the C-terminal helix is investigated.

RESULTS AND DISCUSSION

Ion−Peptide Association from Molecular Dynamics Simulations. At a given temperature (Figure 1, 10 °C), the sequence dependence of ion−peptide association follows expectation. The wild-type peptide has both positively and negatively charged residues; thus, both sodium and chloride associate to a notable degree. The mutant, by contrast, has only negatively charged residues, and therefore, only sodium ions accumulate significantly.

The temperature dependence of the salt−peptide association largely follows the trend suggested by the hypothesis (*9*) that motivated this study. For the wild-type system, sodium ions weakly associate with the peptide; the integrated ion radial distribution function relative to the peptide surface $[N(r)]$ reaches ~1.0 when $r = 3.0$ Å in the 10 °C simulation and decreases to ~0.5 at the same distance in the 45 °C simulation (Figure 2a; for the convergence behavior of $N(r)$, see the Supporting Information). For chloride−peptide association, the value of $N(r)$ seems lower than that for sodium up to $r = 6.0$ Å in the 10 °C simulation and shows very little variation (slight increase) as the temperature increases to 45 °C (Figure 2b).

For the mutant peptide, since there are no positively charged residues, there is little chloride−peptide association (Figure 1b). At 10 °C, the sodium−peptide $N(r)$ at short distances is slightly lower than that calculated for the wild-type peptide (compare Figure 3a and Figure 2a). Remarkably, the temperature dependence of $N(r)$ for the mutant is "normal"; i.e., the $N(r)$ increases as the temperature increases to 45 °C (Figure 3a). We note that the different temperature dependence of ion−peptide association cannot be reproduced in Poisson−Boltzmann calculations where both solvent and ions are treated implicitly (see below).

With regard to the ion association at a given temperature, it is somewhat surprising that chloride association is consistently weaker than sodium association regardless of the peptide sequence because sodium ion has a larger solvation free energy than chloride and therefore is expected to prefer

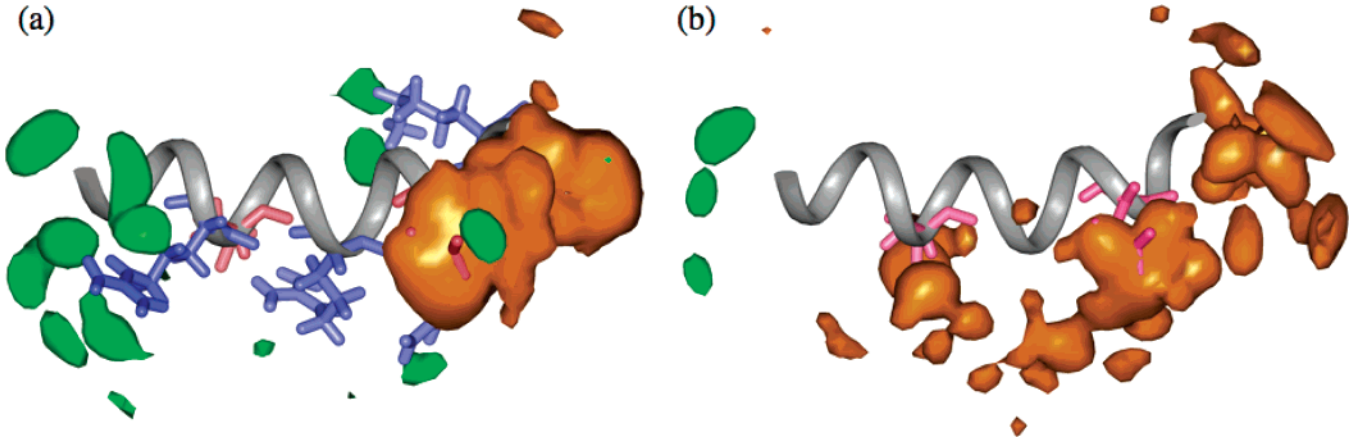

FIGURE 1: Three-dimensional ion density contours around the (a) wild-type and (b) mutant C-terminal helix of hLtn from MD simulations at 10 °C. Chloride and sodium are colored green and orange, respectively; positively and negatively charged residues are colored blue and red, respectively. The density cutoff is 0.8 ion/nm^3.

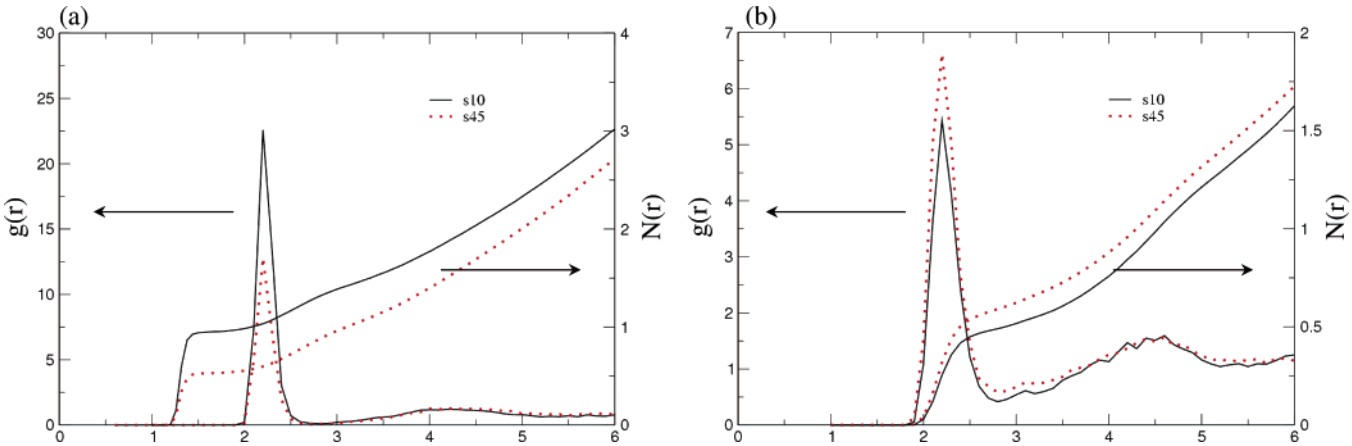

FIGURE 2: Radial distribution function, $g(r)$, of ions with respect to the peptide surface, and its integration, $N(r)$, for the wild-type C-terminal helix of hLtn at 10 and 45 °C from MD simulations: (a) sodium and (b) chloride. Labels s10 and s45 refer to 200 mM NaCl at 10 and 45 °C, respectively. Note the difference in the *y*-axis scales.

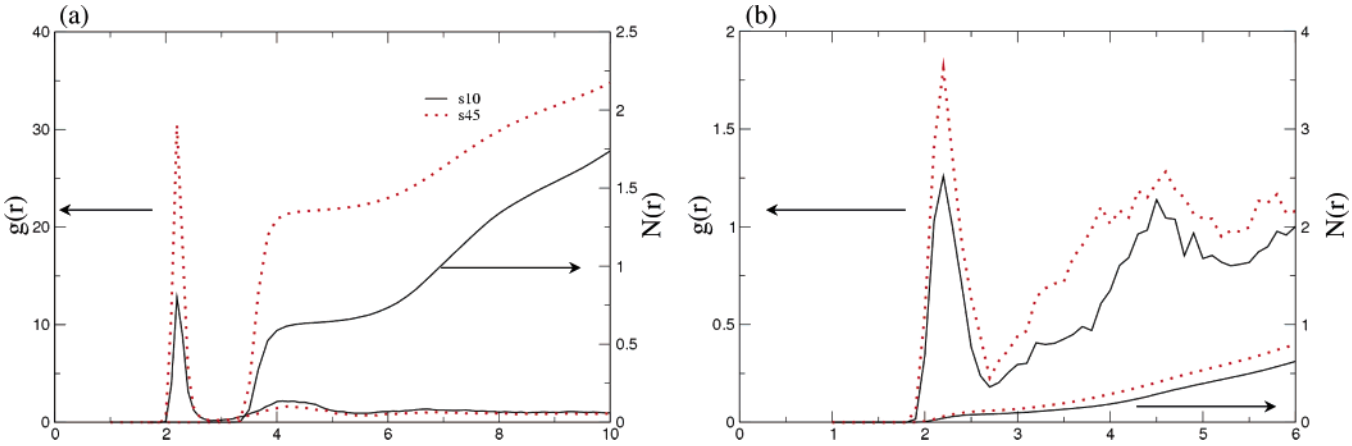

FIGURE 3: Radial distribution function, $g(r)$, of ions with respect to the peptide surface, and its integration, $N(r)$, for the mutant C-terminal helix of hLtn at 10 and 45 °C from MD simulations: (a) sodium and (b) chloride. Labels s10 and s45 refer to 200 mM NaCl at 10 and 45 °C, respectively. Note the difference in the *y*-axis scales.

a solvated environment (*22*−*25*). This might reflect a deficiency of the current CHARMM force field for ions, and it would be of particular interest in the future to compare results to simulations using polarizable force fields (*26*, *27*).

With regard to the different temperature dependence on the sodium−peptide association, since the structure of the peptide is held to be rather rigid except for the fully flexible side chains, the drastically different temperature dependence of ion−peptide association in the wild-type and mutant systems has to be caused by sequence variation. In our previous study (*9*), we noted that the C-terminal helix is clustered with both positively and negatively charged residues; accordingly, the unexpected temperature dependence of ion accumulation in this region was rationalized qualitatively on the basis of the association entropy of charged species in solution. For example, previous integral

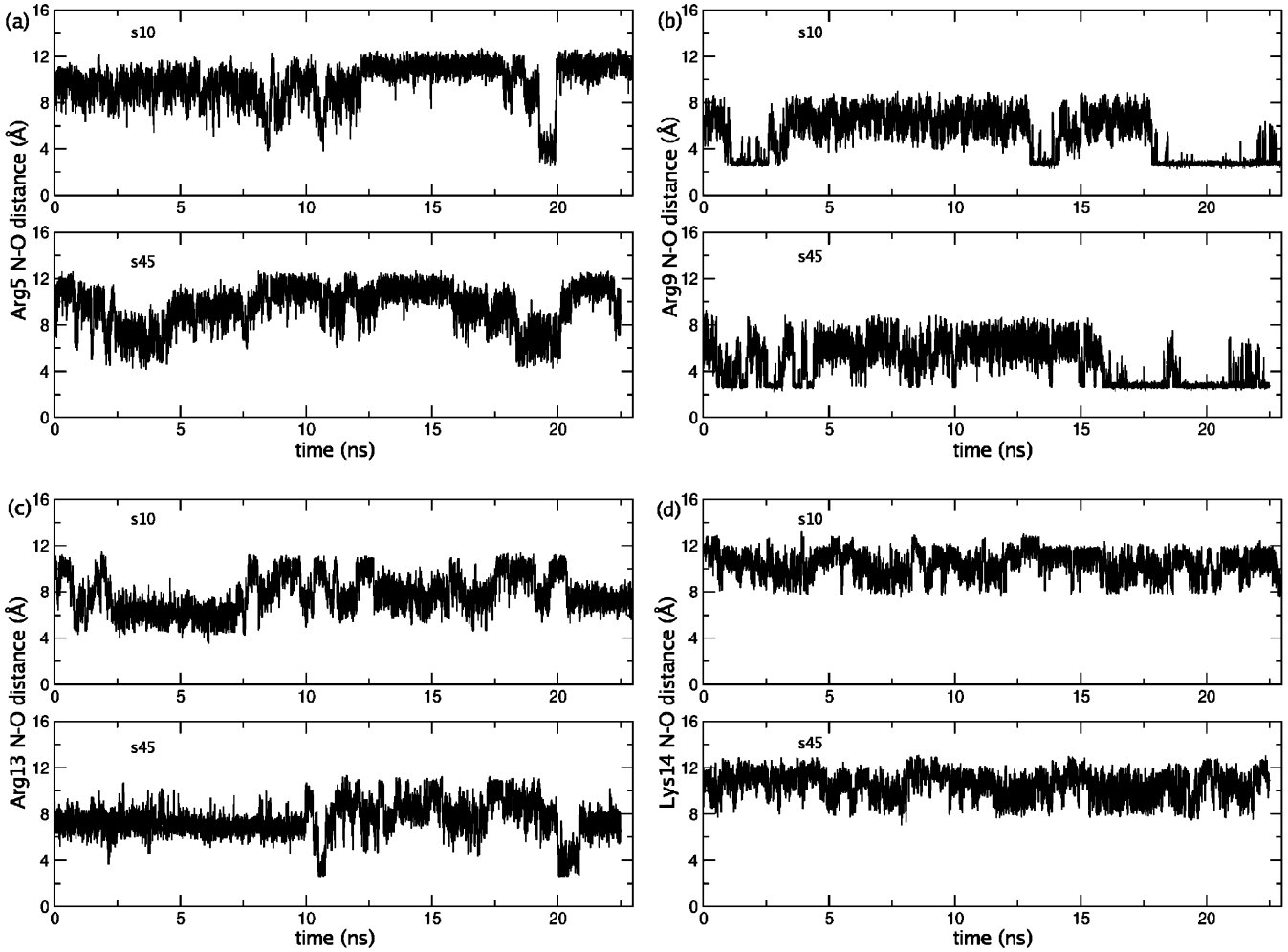

FIGURE 4: Minimal N−O distance (see the text) between four positively charged side chains and all negatively charged side chains (including the C-terminus) along the simulation trajectory for the wild-type peptide at different temperatures: (a) Arg5, (b) Arg9, (c) Arg13, and (d) Lys14. Labels s10 and s45 refer to 200 mM NaCl at 10 and 45 °C, respectively.

equation analysis (*28*) showed that the association of opposite-charge species in solution has a significant entropic driving force since release of water during the association process is entropically favorable. Association of like-charge species, by contrast, has a significant enthalpic driving force and is entropically unfavorable, since the enhanced local electric field upon association restricts the mobility of nearby water molecules. In fact, these trends are easy to see qualitatively from the perspective of continuum electrostatics in which the potential of mean force and entropy for ion (A,B) association have simple forms

$$W(r;T) = q_A q_B/[\epsilon(T) r_{AB}] \quad (3a)$$

$$S(r;T) = -\partial W/\partial T = q_A q_B/[\epsilon^2(T) r_{AB}]\ \partial\epsilon(T)/\partial T \quad (3b)$$

Since the temperature derivative of the water dielectric constant is negative, the entropy of association is positive for opposite-charge species but negative for like-charge species.

Since the hLtn C-terminal peptide is clustered with five positively charged groups and three negatively charged groups (including the N- and C-termini), the negative association entropies between sodium ions and positively charged groups overwhelm the positive association entropies between sodium and negatively charged groups, resulting in weakened sodium−peptide association as the temperature increases. For chloride ions, there are only three like-charge groups but five opposite-charge groups in the wild-type peptide, and therefore, the normal temperature dependence is maintained; the presence of the like-charge groups nevertheless makes the temperature dependence very weak. In the mutant peptide without any positively charged side chains, larger and normal temperature dependence for sodium−peptide association is expected and observed.

Although the argument described above seems to explain the qualitative findings from the simulations, it is important to realize that the decomposition of protein−ion association into the entalphic and entropic components is complex at a quantitative level. Even for the interaction between simple ions in solution, it is well-established that enthalpic and entropic components vary as a function of the interionic distances (*29*). It is perhaps possible to perform a deeper analysis in terms of the Kirkwood−Buff integrals (*30*, *31*), which we leave to future work. More importantly, it is worth pointing out (as emphasized by an anonymous referee) that many processes in a multicomponent solution may be sensitive to temperature. Therefore, it is of interest to examine whether the unexpected temperature dependence of sodium−peptide association in fact reflects other processes such as

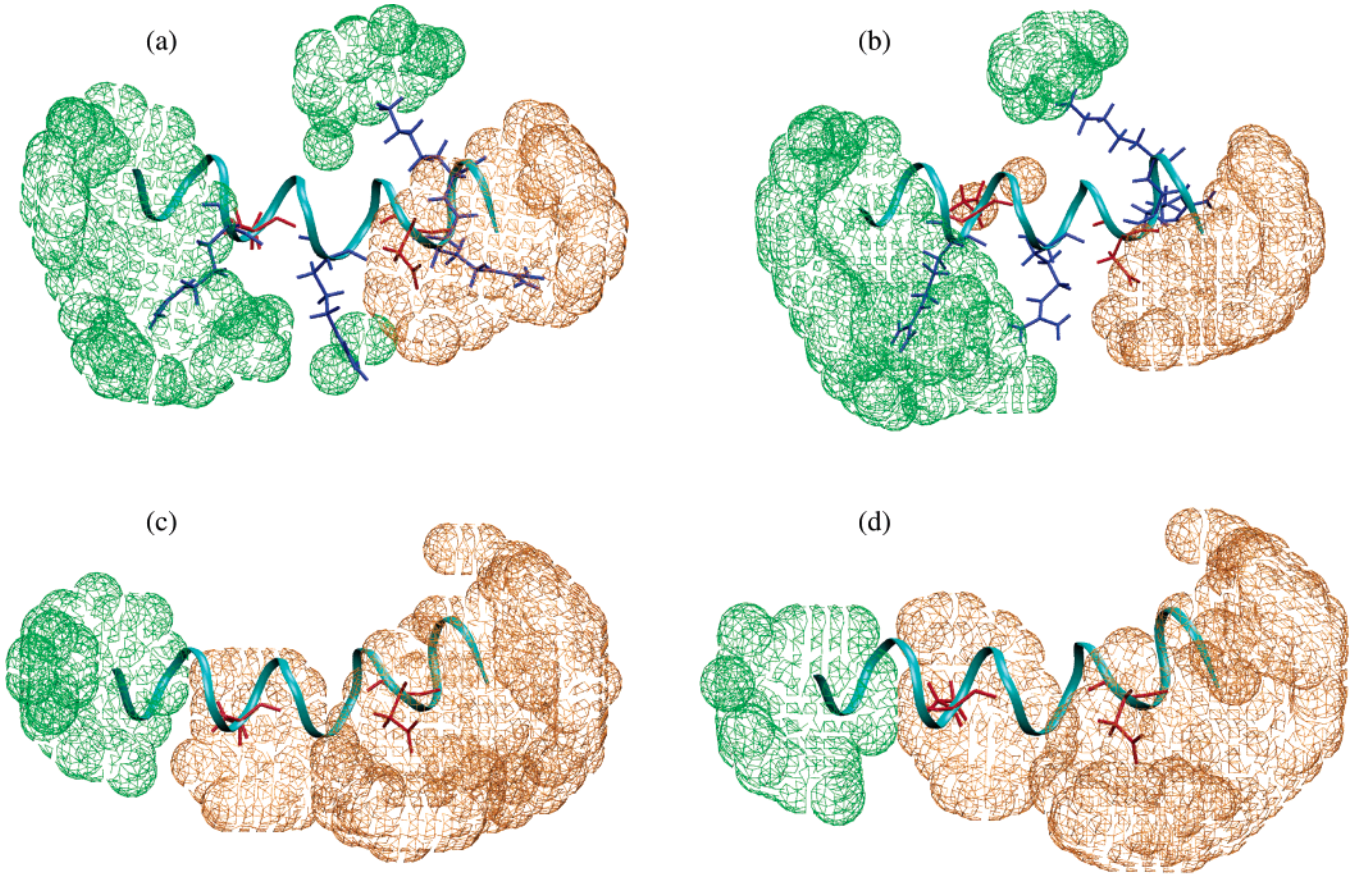

FIGURE 5: Ion distribution difference $\Delta\rho_{Na^+/Cl^-}$ ($\rho_{45°C} - \rho_{10°C}$) by nonlinear PB calculations around (a) a wild-type peptide snapshot from s10 simulation, (b) a wild-type peptide snapshot from s45 simulation, (c) a mutant peptide snapshot from s10 simulation, and (d) a mutant peptide snapshot from s45 simulation. The sodium density increase is colored orange, and the chloride density increase is colored green. The density difference cutoff is $0.1\rho_\infty$ for both ions.

Homo Sapiens	A	T	W	V	R	D	V	V	R	S	M	D	R	K	S	N
					+	−			+			−	+	+		
Pan troglodytes	A	T	W	V	R	D	V	V	R	S	M	D	R	K	S	N
					+	−			+			−	+	+		
Macaca mulatta	A	R	W	V	K	D	V	V	K	S	M	D	R	K	S	N
		+			+	−			+			−	+	+		
Mus musculus	A	K	W	V	K	A	A	I	K	T	V	D	G	R	A	S
		+			+				+			−		+		
Rattus norvegicus	A	K	W	V	K	T	A	I	K	T	V	D	G	R	A	S
		+			+				+			−		+		
Bos taurus	A	A	W	V	K	K	A	V	Q	K	I	D	−	−	−	−
					+	+				+		−				
Ovis aries	V	E	W	V	K	K	A	V	Q	T	I	D	K	−	−	S
		−			+	+						−	+			
Gallus gallus	Q	K	W	V	Q	S	A	M	K	R	I	D	R	R	R	T
		+							+	+		−	+	+	+	

FIGURE 6: Multiple-sequence alignment for several hLtn orthologs in different organisms. Only the C-terminal helix region is shown. Positively charged residues are colored blue and underscored with a plus sign and negatively charged residues colored red and underscored with a minus sign.

sodium−chloride association and salt bridge formation between peptide side chains.

As shown in the Supporting Information, the sodium−chloride association exhibits the expected temperature dependence in both the wild-type and mutant peptide simulations. With regard to the salt bridge dynamics associated with the wild-type peptide side chains (no salt bridge is possible in the mutant), the minimal distance between four positively charged side chains and all negatively charged side chains (including the C-terminus) is monitored throughout the simulation. The salt bridge is regarded as being formed if the distance between the nitrogen atom of positively charged residues (NH1 and NH2 for Arg and NZ for Lys) and the oxygen atom of negatively charged residues (OD1 and OD2 for Asp and Glu and OT1 and OT2 for the C-terminus) is less than 4.0 Å (*32*). It is shown in Figure 4 that Lys14 is not involved in any salt bridge, whereas Arg5 and Arg13 form salt bridges only sporadically (several hundred picoseconds out of ~23 ns). Arg9 is the only positively charged residue that forms relatively stable salt bridges (with Asp6) at both temperatures. The interaction appears stronger at the higher temperature on the basis of the lifetime of the salt bridge interactions, although it is difficult to quantify with only ~23 ns simulations. Nevertheless, we note that the salt bridge between Arg9 and Asp6 is mainly formed after 12 ns, when the distribution of sodium and chloride ions around the peptide has largely converged (see the convergence plot in the Supporting Information), implying that the formation of a salt bridge does not have a major effect on the salt−peptide association in our simulations. In short, we conclude that neither sodium chloride association nor salt bridge dynamics is a major factor that leads to the unexpected temperature dependence of sodium−peptide association in the wild-type system, which further supports our hypothesis (*9*) based on the association entropies of different ionic pairs in solution.

Ion−Peptide Association from Nonlinear PB Calculations. The temperature dependences of the ion distribution around the wild-type peptide and the mutant peptide from PB calculations are shown in Figure 5. As the temperature increases from 10 to 45 °C, both ions accumulate more around both peptides. Since peptide backbones are held rigid during simulations, only results for two snapshots for each peptide are shown (though calculations averaged over snapshots are done and the results are similar). Clearly, PB calculations cannot reproduce the abnormal temperature dependence of ion distribution around the wild-type peptide since PB treats the solvent as a dielectric continuum without properly taking into account the solvent entropy. Therefore, the different temperature dependence for ion−peptide association in the wild-type and mutant peptides cannot be understood as a result of the difference in the net charge (+2 vs −2) and further supports our entropy-based explanation. We emphasize that the failure of PB in this case is likely due to the implicit treatment of the ions in solution. Indeed, as shown in the Supporting Information, PB calculations can successfully capture the different temperature dependence for the interaction between ion−side chain pairs of different charges, provided that the ion is represented explicitly and the temperature dependence of the water dielectric is taken into account (*10*). In other words, there is no conflict between the failure of PB as illustrated in Figure 5 and using eq 3 to rationalize the sign of association entropy for different ion−side chain pairs.

Multiple-Sequence Alignment. All the trends observed in the current set of MD simulations can be explained by considering the association entropy of charged species in solution, which highlights the importance of local sequence in determining the temperature dependence of ion−protein association. Whether hLtn takes advantage of this interesting behavior for its function remains debatable, although it is interesting to note that the result of multiple-sequence alignment reveals that the feature of alternating positively and negatively charged residues in the C-terminal region is conserved among several lymphotactin family members (Figure 6), which seems to imply that this design is related to the stability and function of hLtn. However, it may also simply reflect the fact that dimerization, which was found to be sensitive to temperature and salt concentration (*8*), has an important electrostatic component (*9*).

CONCLUDING REMARKS

Using the C-terminal helix of hLtn and its designed mutant, we show that the temperature dependence of ion−protein association is highly dependent on the distribution of charged residues. This sequence specificity can be qualitatively explained by taking into account the association entropy of charged species in solution and cannot be captured by PB calculations that treat solvent and ions in an implicit manner. The association between sodium chloride ions in solution and the salt bridge dynamics in the wild-type peptide also exhibits temperature dependence, although neither is likely to have a major influence on the ion−peptide association in these simulations.

Although this work focuses on protein−salt association, our discussion of the association entropy of charged species has general implications for bimolecular association involving significant electrostatic components, such as protein−DNA interactions (*33*). For example, since ion release upon binding is an important component in binding thermodynamic quantities such as heat capacity change (*1*−*7*), the finding that the ion distribution around the protein may have variable temperature dependence sensitive to the local sequence suggests that additional complexity may arise that further complicates the thermodynamic analysis. Finally, we encourage direct experimental probing of ion−protein association as functions of temperature and local sequence, which might be possible with recent developments in X-ray spectroscopy techniques using liquid microjets (*34*).

ACKNOWLEDGMENT

Computational resources from the National Center for Supercomputing Applications at the University of Illinois are greatly appreciated. Discussions with Profs. M. T. Record, Jr., B. Volkman, A. Yethiraj, and N. Baker are greatly appreciated.

SUPPORTING INFORMATION AVAILABLE

Convergence analysis for the ion accumulation around the peptide, results for the association between sodium and chloride ions and implicit solvent model calculations for the binding free energy between ions and charged sidechains as a function of temperature are reported. This material is available free of charge via the Internet at http://pubs.acs.org.

REFERENCES

1. Wyman, J. (1964) Linked functions and reciprocal effects in hemoglobin: A second look, *Adv. Protein Chem. 19*, 223−286.
2. Volker, J., and Breslauer, K. J. (2005) Communication between noncontacting macromolecules, *Annu. Rev. Biophys. Biomol. Struct. 34*, 21−42.
3. Record, M. T., Zhang, W. T., and Anderson, C. F. (1998) Analysis of effects of salts and uncharged solutes on protein and nucleic acid equilibria and processes: A practical guide to recognizing and interpreting polyelectrolyte effects, Hofmeister effects, and osmotic effects of salts, *Adv. Protein Chem. 51*, 281−353.
4. Timasheff, S. N. (1998) Control of protein stability and reactions by weakly interacting cosolvents: The simplicity of the complicated, *Adv. Protein Chem. 51*, 355−432.
5. Schellman, J. A. (1978) Solvent denaturation, *Biopolymers 17*, 1305−1322.
6. Hribar, B., Southall, N. T., Vlachy, V., and Dill, K. A. (2002) How ions affect the structure of water, *J. Am. Chem. Soc. 124*, 12302−12311.
7. Courtenay, E. S., Capp, M. W., Anderson, C. F., and Record, M. T. (2000) Vapor pressure osmometry studies of osmolyte-protein interactions: Implications for the action of osmoprotectants in vivo and for the interpretation of "osmotic stress" experiments in vitro, *Biochemistry 39*, 4455−4471.
8. Kuloglu, E. S., McCaslin, D. R., Markley, J. L., and Volkman, B. F. (2002) Structural rearrangement of human lymphotactin, a c chemokine, under physiological solution conditions, *J. Biol. Chem. 277*, 17863−17870.
9. Formaneck, M. S., Ma, L., and Cui, Q. (2006) Effects of temperature and salt concentration on the structural stability of human lymphotactin: Insights from molecular simulations, *J. Am. Chem. Soc. 128*, 9506−9517.
10. Elcock, A. H., and McCammon, J. A. (1997) Continuum solvation model for studying protein hydration thermodynamics at high temperatures, *J. Phys. Chem. B 101*, 9624−9634.
11. Brooks, B. R., Bruccoleri, R. E., Olafson, B. D., States, D. J., Swaminathan, S., and Karplus, M. (1983) Charmm: A program for macromolecular energy, minimization, and dynamics calculations, *J. Comput. Chem. 4*, 187−217.
12. Ryckaert, J. P., Ciccotti, G., and Berendsen, H. J. C. (1977) Numerical-integration of cartesian equations of motion of a system with constraints: Molecular dynamics of n-alkanes, *J. Comput. Phys. 23*, 327−341.

13. Steinbach, P. J., and Brooks, B. R. (1994) New spherical-cutoff methods for long-range forces in macromolecular simulation, *J. Comput. Chem. 15*, 667−683.
14. Darden, T., York, D., and Pedersen, L. (1993) Particle mesh ewald: An n.Log(n) method for Ewald sums in large systems, *J. Chem. Phys. 98*, 10089−10092.
15. Nose, S. (1984) A unified formulation of the constant temperature molecular-dynamics methods, *J. Chem. Phys. 81*, 511−519.
16. Hoover, W. G. (1985) Canonical dynamics: Equilibrium phase-space distributions, *Phys. Rev. A 31*, 1695−1697.
17. Feller, S. E., Zhang, Y. H., Pastor, R. W., and Brooks, B. R. (1995) Constant-pressure molecular-dynamics simulation: The Langevin piston method, *J. Chem. Phys. 103*, 4613−4621.
18. Andersen, H. C. (1980) Molecular-dynamics simulations at constant pressure and/or temperature, *J. Chem. Phys. 72*, 2384−2393.
19. Nina, M., Beglov, D., and Roux, B. (1997) Atomic radii for continuum electrostatics calculations based on molecular dynamics free energy simulations, *J. Phys. Chem. B 101*, 5239−5248.
20. MacKerell, A. D., Bashford, D., Bellott, M., Dunbrack, R. L., Evanseck, J. D., Field, M. J., Fischer, S., Gao, J., Guo, H., Ha, S., Joseph-McCarthy, D., Kuchnir, L., Kuczera, K., Lau, F. T. K., Mattos, C., Michnick, S., Ngo, T., Nguyen, D. T., Prodhom, B., Reiher, W. E., Roux, B., Schlenkrich, M., Smith, J. C., Stote, R., Straub, J., Watanabe, M., Wiorkiewicz-Kuczera, J., Yin, D., and Karplus, M. (1998) All-atom empirical potential for molecular modeling and dynamics studies of proteins, *J. Phys. Chem. B 102*, 3586−3616.
21. Edgar, R. C. (2004) Muscle: Multiple sequence alignment with high accuracy and high throughput, *Nucleic Acids Res. 32*, 1792−1797.
22. Marcus, Y. (1986) The Hydration Entropies of Ions and Their Effects on the Structure of Water, *J. Chem. Soc., Faraday Trans. 1 82*, 233−242.
23. Gomer, R., and Tryson, G. (1977) Experimental-Determination of Absolute Half-Cell Emfs and Single Ion Free-Energies of Solvation, *J. Chem. Phys. 66*, 4413−4424.
24. Klots, C. E. (1981) Solubility of Protons in Water, *J. Phys. Chem. 85*, 3585−3588.
25. Tissandier, M. D., Cowen, K. A., Feng, W. Y., Gundlach, E., Cohen, M. H., Earhart, A. D., Coe, J. V., and Tuttle, T. R. (1998) The proton's absolute aqueous enthalpy and Gibbs free energy of solvation from cluster-ion solvation data, *J. Phys. Chem. A 102*, 7787−7794.
26. Lamoureux, G., and Roux, B. (2006) Absolute hydration free energy scale for alkali and halide ions established from simulations with a polarizable force field, *J. Phys. Chem. B 110*, 3308−3322.
27. Grossfield, A., Ren, P. Y., and Ponder, J. W. (2003) Ion solvation thermodynamics from simulation with a polarizable force field, *J. Am. Chem. Soc. 125*, 15671−15682.
28. Yu, H. A., Roux, B., and Karplus, M. (1990) Solvation Thermodynamics: An Approach from Analytic Temperature Derivatives, *J. Chem. Phys. 92*, 5020−5032.
29. Pettitt, B. M., and Rossky, P. J. (1986) Alkali-Halides in Water: Ion Solvent Correlations and Ion Ion Potentials of Mean Force at Infinite Dilution, *J. Chem. Phys. 84*, 5836−5844.
30. Kirkwood, J. G., and Buff, F. P. (1951) The statistical mechanical theory of solutions. I, *J. Chem. Phys. 19*, 774−777.
31. Smith, P. E. (2006) Equilibrium dialysis data and the relationships between preferential interaction parameters for biological systems in terms of Kirkwood-Buff integrals, *J. Phys. Chem. B 110*, 2862−2868.
32. Barlow, D. J., and Thornton, J. M. (1983) Ion Pairs in Proteins, *J. Mol. Biol. 168*, 867−885.
33. Saecker, R. M., and Record, M. T. (2002) Protein surface salt bridges and paths for DNA wrapping, *Curr. Opin. Struct. Biol. 12*, 311−319.
34. Messer, B. M., Cappa, C. D., Smith, J. D., Drisdell, W. S., Schwartz, C. P., Cohen, R. C., and Saykally, R. J. (2005) Local hydration environments of amino acids and dipeptides studied by X-ray spectroscopy of liquid microjets, *J. Phys. Chem. B 109*, 21640−21646.

BI0613067